crystals

MDPI

Article

Comparative Ab Initio Calculations of ReO_3, $SrZrO_3$, $BaZrO_3$, $PbZrO_3$ and $CaZrO_3$ (001) Surfaces

Roberts I. Eglitis [1,*], Juris Purans [1], Jevgenijs Gabrusenoks [1], Anatoli I. Popov [1] and Ran Jia [1,2]

[1] Institute of Solid State Physics, University of Latvia, 8 Kengaraga Str., LV-1063 Riga, Latvia; purans@cfi.lu.lv (J.P.); gabrusen@latnet.lv (J.G.); popov@ill.fr (A.I.P.); jiaran@jlu.edu.cn (R.J.)

[2] Laboratory of Theoretical and Computational Chemistry, Institute of Theoretical Chemistry, Jilin University, Changchun 130023, China

* Correspondence: rieglitis@gmail.com; Tel.: +371-26426703

Received: 30 June 2020; Accepted: 19 August 2020; Published: 24 August 2020

Abstract: We performed, for first time, ab initio calculations for the ReO_2-terminated ReO_3 (001) surface and analyzed systematic trends in the ReO_3, $SrZrO_3$, $BaZrO_3$, $PbZrO_3$ and $CaZrO_3$ (001) surfaces using first-principles calculations. According to the ab initio calculation results, all ReO_3, $SrZrO_3$, $BaZrO_3$, $PbZrO_3$ and $CaZrO_3$ (001) surface upper-layer atoms relax inwards towards the crystal bulk, all second-layer atoms relax upwards and all third-layer atoms, again, relax inwards. The ReO_2-terminated ReO_3 and ZrO_2-terminated $SrZrO_3$, $BaZrO_3$, $PbZrO_3$ and $CaZrO_3$ (001) surface band gaps at the Γ–Γ point are always reduced in comparison to their bulk band gap values. The Zr–O chemical bond populations in the $SrZrO_3$, $BaZrO_3$, $PbZrO_3$ and $CaZrO_3$ perovskite bulk are always smaller than those near the ZrO_2-terminated (001) surfaces. In contrast, the Re–O chemical bond population in the ReO_3 bulk (0.212*e*) is larger than that near the ReO_2-terminated ReO_3 (001) surface (0.170*e*). Nevertheless, the Re–O chemical bond population between the Re atom located on the ReO_2-terminated ReO_3 (001) surface upper layer and the O atom located on the ReO_2-terminated ReO_3 (001) surface second layer (0.262*e*) is the largest.

Keywords: ab initio methods; ABO_3 perovskites; ReO_3; (001) surface; B3PW; B3LYP

1. Introduction

Forefront (001) surfaces as well as (001) interface phenomena—which occur in the ABO_3 perovskite oxides and ReO_3—are hot topics in modern solid state physics due to their desirable atomic and electronic processes [1–9]. During the last quarter century, due to their great technological importance, as well as a comprehensive fundamental interest, the $SrZrO_3$, $BaZrO_3$, $CaZrO_3$ and $PbZrO_3$ (001) surfaces have been extensively investigated both theoretically and experimentally [10–22]. $SrZrO_3$, $BaZrO_3$, $PbZrO_3$ and $CaZrO_3$ matrices are so-called ABO_3 perovskites, where A = Sr; Ba; Pb; or Ca and B = Zr. ABO_3 perovskites have a large number of industrially important applications, for example, as actuators, capacitors and charge storage devices, etc. [23–27]. For many of those ABO_3 perovskite applications, surface quality and structure play important roles. For example, recent studies have shown that the catalytic properties of ABO_3 perovskite oxides are largely related to oxygen vacancies, which alter their electronic and crystal structures as well as surface chemistry [28–32].

Rhenium trioxide, ReO_3, is often referred to as a covalent metal since it has very high electrical conductivity [33]. The electrical conductivity of ReO_3 is similar to that of silver or copper [33]. Despite the great technological interest, there have been very few ab initio calculations and experimental studies performed on ReO_3 polar (001) surfaces [34–37]. It is worth noting that there have been no ab initio studies performed, to the best of our knowledge, on the atomic relaxation of the ReO_2-terminated polar ReO_3 (001) surface. ReO_3 related materials, such as $LiReO_3$ and Li_2ReO_3, are prospective battery

cathode materials [38]. The predictive power of first-principle calculations allows for the theoretical design of new materials for advanced technology applications. An excellent example is the theoretical prediction of the average voltages for a four-volt battery cathodes from first-principles calculations by Ceder and his coworkers [39,40]. Moreover, recently, based on first-principles calculations, it was shown that a five-volt battery was possible using $Li_2CoMn_3O_8$ as the cathode material [41,42].

In the classical cubic unit cells of $SrZrO_3$, $BaZrO_3$, $PbZrO_3$ and $CaZrO_3$ perovskites, which contain five atoms, the A type atom is located at the cube-corner position with the coordinates (0, 0, 0). The B type atom is located at the body-center position with the coordinates (1/2, 1/2, 1/2). Finally, the three O atoms are located at face-centered positions equal to (1/2, 1/2, 0), (1/2, 0, 1/2) and (0, 1/2, 1/2). The ABO_3 perovskite's A atom is always considerably larger than its B atom. All cubic ABO_3 perovskites belong to the *P*m3m space group, for which the space group number is 221. ReO_3 forms the crystallizes in the cubic ABO_3 perovskite structure—*P*m3m space group and space group number 221—with the only difference being the unoccupied A-cation site [37].

The goal of the work reported in this paper is to perform, for the first time, ab initio calculations for polar ReO_2-terminated ReO_3 (001) surfaces. The ab initio calculation results for the polar ReO_2-terminated ReO_3 (001) surface were compared with the calculation results for neutral ZrO_2-terminated $SrZrO_3$, $BaZrO_3$, $PbZrO_3$ and $CaZrO_3$ (001) surfaces. The calculation results for all five materials were carefully analyzed and systematic trends common for all ReO_3, $SrZrO_3$, $BaZrO_3$, $PbZrO_3$ and $CaZrO_3$ (001) surfaces were elucidated and are reported herein.

2. Computational Method

We performed ab initio calculations for the ReO_3, $SrZrO_3$, $BaZrO_3$, $PbZrO_3$ and $CaZrO_3$ bulk and ReO_2 or ZrO_2-terminated (001) surfaces, respectively, using the hybrid exchange–correlation functionals B3PW [43] or B3LYP [44] as well as the widely recognized CRYSTAL computer code [45]. The $SrTiO_3$ [46], CaF_2 [47] and MgF_2 [48] bulk Γ–Γ band gaps that were calculated using different exchange–correlation functionals are provided in Table 1. The experimentally measured $SrTiO_3$ [49], CaF_2 [50] and MgF_2 [51,52] bulk band gaps at the Γ-point are listed in Table 1 for the purpose of comparison. It is well known that the local-density approximations (LDA) and generalized-gradient approximations (GGA) used in density functional theory (DFT) systematically underestimate the band gap in complex oxide materials, such as ABO_3 perovskites and insulators by a factor of almost two (Table 1). In contrast, it is well known that the Hartree–Fock (HF) method systematically overestimates the band gap of solids. With the aim of generating a reliable basis for further ABO_3 perovskites and ReO_3 bulk and (001) surface calculations, which require a precise description of the Γ–Γ band gap, we performed the ReO_3, $SrZrO_3$, $BaZrO_3$, $PbZrO_3$ and $CaZrO_3$ bulk and (001) surface calculations by means of the hybrid exchange–correlation functionals B3PW or B3LYP, which utilize 20% of the HF method and 80% of the DFT Hamiltonian method when implemented in the CRYSTAL computer package [45].

Table 1. $SrTiO_3$, CaF_2 and MgF_2 bulk Γ–Γ band gaps calculated using different exchange–correlation functionals. Experimental bulk band gap data at the Γ-point are listed for comparison.

Method	$SrTiO_3$ [46]	CaF_2 [47]	MgF_2 [48]
Experiment	**3.75 [49]**	**12.1 [50]**	**12.4 [51]; 13.0 [52]**
B3PW	3.96	10.96	9.48
B3LYP	3.89	10.85	9.42
HF	12.33	20.77	19.65
PWGGA	2.31	8.51	6.94
PBE	2.35	8.45	6.91

For example, as can be seen from Table 1, the ab initio HF calculations strongly overestimate the experimental $SrTiO_3$ bulk band gap at the Γ-point—by 3.29 times. In contrast, the DFT-based

PWGGA and PBE exchange–correlation functionals considerably underestimate the experimental $SrTiO_3$ band gap at the Γ-point—by 1.62 and 1.60 times, respectively. Finally, the B3PW and B3LYP hybrid-exchange correlation functionals only slightly overestimate the experimental $SrTiO_3$ band gap at the Γ-point—by 1.06 and 1.04 times, respectively. For predominantly this reason, the B3PW and B3LYP hybrid exchange–correlation functionals were used in all subsequent ReO_3, $SrZrO_3$, $BaZrO_3$, $PbZrO_3$ and $CaZrO_3$ bulk and (001) surface ab initio calculations performed by means of the CRYSTAL computer code [45].

The key power of the CRYSTAL computer code, which is important for the study of neutral $SrZrO_3$, $BaZrO_3$, $PbZrO_3$ and $CaZrO_3$ as well as polar ReO_3 (001) surfaces, is its use of the 2D isolated slab model, without artificial repetition along the *z*-axis. The reciprocal space integration, in the ab initio calculations, were performed by sampling the Brillouin zone with an $8 \times 8 \times 1$ times extended Pack–Monkhorst mesh for the ReO_3, $SrZrO_3$, $BaZrO_3$, $PbZrO_3$ and $CaZrO_3$ (001) surfaces and $8 \times 8 \times 8$ mesh for the bulk of those materials. In order to achieve highly accurate calculations, large enough tolerances of 7, 8, 7, 7 and 14 were chosen for the Coulomb overlap, Coulomb penetration, exchange overlap, first-exchange pseudo-overlap and second-exchange pseudo-overlap, respectively [45].

In order to calculate the neutral BO_2-terminated ABO_3 perovskite (001) surfaces (Figure 1), we used symmetrical slabs consisting of nine, neutral, alternating BO_2 or AO layers perpendicular to the [001] crystal direction [11,14,16,41]. The slabs were rotated to make them perpendicular to the Oz axis. The CRYSTAL computer package [45] made it possible to avoid artificial periodicity along the Oz direction and to perform calculations for stand-alone 2D slabs. Taking into account the classical ionic charges for A(+2*e*), for B(+4*e*) and for O(−2*e*), both the AO and BO_2 layers have a formal ionic charge equal to zero. The nine-layer slab, used in ABO_3 perovskite (001) surface calculations, was terminated on both sides by BO_2 planes and thereby consisted of a 23-atom supercell (Figure 1). The calculated BO_2-terminated ABO_3 perovskite (001) slabs were non-stoichiometric, with an empirical unit cell of $A_4B_5O_{14}$ [11,14,16,41].

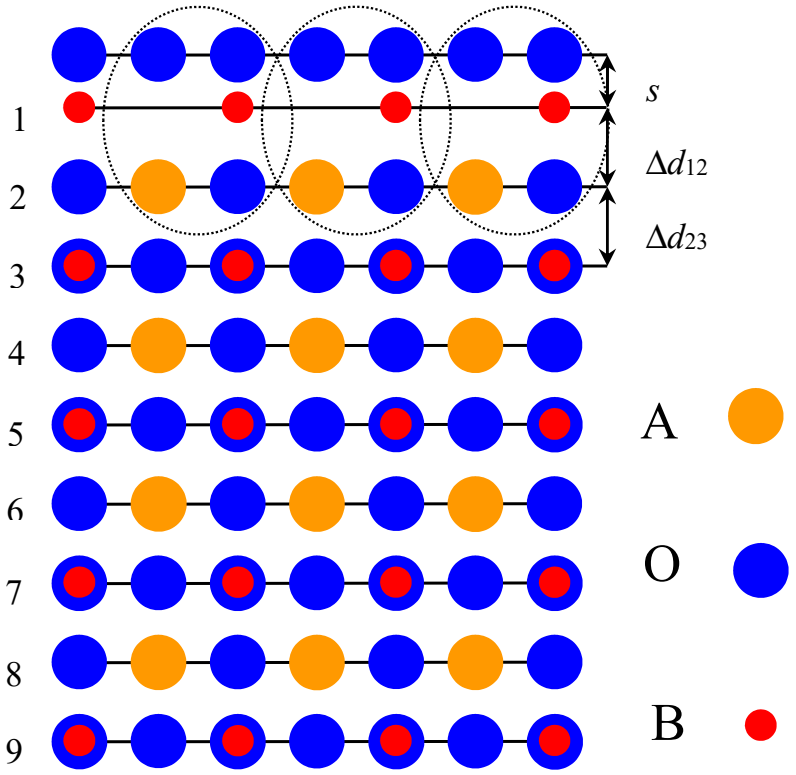

Figure 1. Side-view of the nine-layer BO_2-terminated ABO_3 perovskite (001) surface.

In contrast to neutral ABO_3 perovskite (001) surfaces, it is much more difficult to calculate polar, ReO_2-terminated ReO_3 (001) surfaces, which consist of charged ReO_2 and O layers, taking into account the classical ionic charges of Re(+6*e*) and O(−2*e*) (Figure 2). Furthermore, for the ReO_2-terminated polar ReO_3 (001) surface calculations, we used symmetrical nine-layer slabs, which consisted of polar, alternating ReO_2 and O layers and contained 19 atoms, with an empirical unit cell of B_5O_{14}. The nine-layer ReO_2-terminated ReO_3 surface, taking into account formal ionic charges (ReO_2(+2*e*)–O(−2*e*)–ReO_2(+2*e*)–O(−2*e*)–ReO_2(+2*e*)–O(−2*e*)–ReO_2(+2*e*)–O(−2*e*)–ReO_2(+2*e*)), has a positive charge equal to +2*e*. In all calculations performed by CRYSTAL computer code, the unit cell should be neutral. In order to make the calculations feasible, for polar ReO_2-terminated ReO_3 (001) surfaces, instead of ionic basis sets—as in case of ABO_3 perovskites—the basis sets for neutral Re and O atoms were used. For example, for the O atom, the basis sets developed by Piskunov et al. [46] were used, and two electrons were removed from the O^{2-} ion to obtain the basis set for the neutral O atom [5,53,54]. For the Re atom, we used the basis set developed by Cora [45]. Using the atomic basis sets for Re and O atoms, we obtained the polar ReO_2-terminated ReO_3 (001) surface with a formal charge equal to 0, and thereby, such calculations are feasible with the CRYSTAL computer code. As we know from previous studies, on, for example, with polar $CaTiO_3$ and $SrTiO_3$ (111) surfaces [55–59], a very strong electron redistribution is observed, which deletes the polarity effects. It is evident that it is impossible to calculate the asymmetric slabs with different terminations, such as ReO_2–O–ReO_2—-O–ReO_2–O–ReO_2–O, since, in the case for the asymmetric slab, it has a large dipole moment perpendicular to the ReO_2-terminated ReO_3 crystal (001) surface.

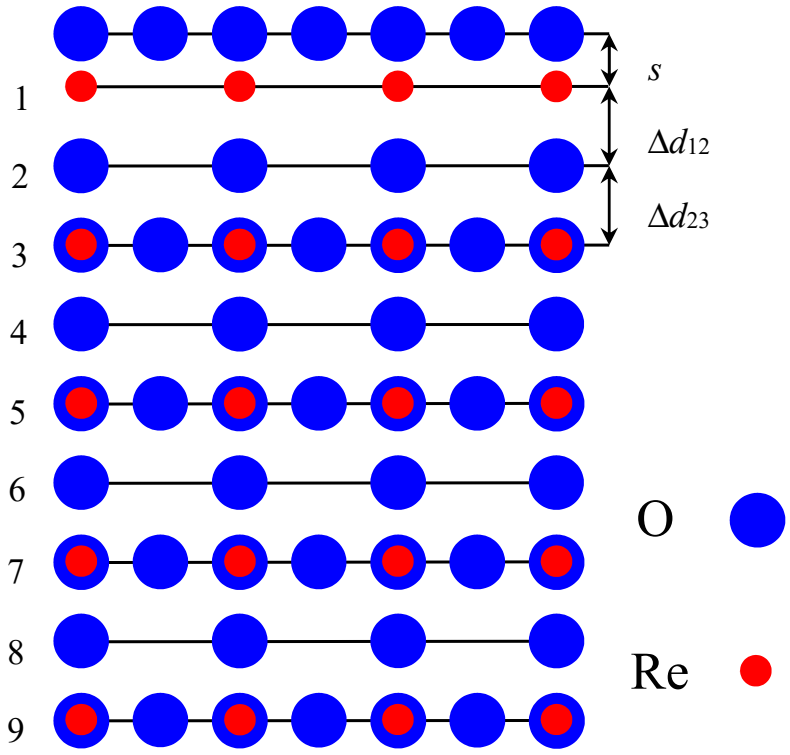

Figure 2. Side-view of the nine-layer ReO_2-terminated ReO_3 polar (001) surface.

To correctly describe the chemical bonding as well as covalency effects for both ReO_3, $SrZrO_3$, $BaZrO_3$, $PbZrO_3$, $CaZrO_3$ bulk and their (001) surfaces, we used a standard Mulliken population analysis as it is implemented in the CRYSTAL computer code [45]. Namely, the Mulliken population analysis was used for the chemical bond populations *P*, effective atomic charges *q*, as well as another local properties of the ReO_3, $SrZrO_3$, $BaZrO_3$, $PbZrO_3$ and $CaZrO_3$ electronic structure, such as the bond orders, atomic covalences and full valences [60–62].

3. Numeric Results of ReO_3, $SrZrO_3$, $BaZrO_3$, $PbZrO_3$, $CaZrO_3$ Bulk and (001) Surface Calculations

3.1. Ab Initio Calculations of ReO_3, $SrZrO_3$, $BaZrO_3$, $PbZrO_3$ and $CaZrO_3$ Bulk Properties

In order to begin the calculations, by means of the B3LYP or B3PW functional, the ReO_3, $SrZrO_3$, $BaZrO_3$, $PbZrO_3$ and $CaZrO_3$ bulk lattice constants were calculated and compared with actual experimental data (Table 2). As shown in Table 2, the B3LYP calculated ReO_3 bulk lattice constant (3.758 Å) is only overestimated by 0.29% with respect to the experimental value of 3.747 Å [63]. The, by means of hybrid exchange–correlation functionals, calculated $SrZrO_3$, $BaZrO_3$ and $PbZrO_3$ bulk lattice constants are overestimated with respect to the experimentally measured bulk lattice constants by 0.99%, 0.83% and 1.41%, respectively [64–66]. The theoretical ReO_3, $SrZrO_3$, $BaZrO_3$, $PbZrO_3$ and $CaZrO_3$ [67] bulk lattice constants were used in all subsequent (001) surface calculations.

Table 2. B3LYP or B3PW calculated ReO_3, $SrZrO_3$, $BaZrO_3$, $PbZrO_3$ and $CaZrO_3$ bulk lattice constants (in Å). The experimental bulk lattice constants are listed for the purpose of comparison.

Crystal	Functional	Theory	Experiment
ReO_3	B3LYP	3.758	3.747 [63]
$SrZrO_3$	B3LYP	4.195 [14]	4.154 [64]
$BaZrO_3$	B3PW	4.234 [11]	4.199 [65]
$PbZrO_3$	B3LYP	4.220 [14]	4.1614 [66]
$CaZrO_3$	B3LYP	4.157 [67]	No data for cubic phase

The calculated effective charge is +2.382*e* for the Re atom in the ReO_3 bulk matrix (Table 3). The calculated Zr effective charges in the $SrZrO_3$, $BaZrO_3$, $PbZrO_3$ and $CaZrO_3$ perovskites (+2.174*e*, +2.134*e*, +2.111*e* and +2.144*e*, respectively) are similar to each other and strongly different from the Zr formal ionic charge (+4*e*). The calculated O effective charge in the ReO_3 bulk is equal to −0.794*e*. Ab initio calculated O effective charges in the $SrZrO_3$, $BaZrO_3$, $PbZrO_3$ and $CaZrO_3$ perovskites are equal to −1.351*e*, −1.316*e*, −1.160*e* and −1.310*e*, respectively. Therefore, the $SrZrO_3$, $BaZrO_3$ and $CaZrO_3$ O effective charges are similar, but the O effective charge in the $PbZrO_3$ crystal is considerably smaller, only −1.160*e* (Table 3). The chemical bond population between Re and O atoms in ReO_3 is equal to +0.212*e*. The chemical bond population between Zr and O atoms in $SrZrO_3$, $BaZrO_3$, $PbZrO_3$ and $CaZrO_3$ matrices are equal to +0.092*e*, 0.108*e*, 0.106*e*, 0.086*e*, respectively. Large chemical bond population values between B and O atoms in ReO_3, $SrZrO_3$, $BaZrO_3$, $PbZrO_3$ and $CaZrO_3$ crystals indicate that the chemical bonding in these materials is covalent.

Table 3. By means of the hybrid exchange–correlation functionals B3LYP or B3PW calculated effective atomic charges *Q* and bond populations *P* in ReO_3, $SrZrO_3$, $BaZrO_3$, $PbZrO_3$ and $CaZrO_3$.

Material, Bulk		ReO_3	$SrZrO_3$	$BaZrO_3$	$PbZrO_3$	$CaZrO_3$
Ion	**Property**	**B3LYP**	**B3LYP**	**B3PW**	**B3LYP**	**B3LYP**
A	*Q*	–	+1.880	+1.815	+1.368	+1.787
	P	–	+0.002	−0.012	+0.030	+0.014
O	*Q*	−0.794	−1.351	−1.316	−1.160	−1.310
	P	+0.212	+0.092	+0.108	+0.106	+0.086
B	*Q*	+2.382	+2.174	+2.134	+2.111	+2.144

By means of the B3LYP or B3PW hybrid exchange–correlation functionals, the ReO_3, $SrZrO_3$, $BaZrO_3$, $PbZrO_3$ and $CaZrO_3$ bulk band gaps at the Γ–Γ point were calculated for the cubic phase of these crystals. It is worth mentioning that the hybrid exchange–correlation functionals, such as B3LYP or B3PW are in excellent agreement with the experimentally obtained band gaps of related

ABO_3 perovskites and their (001) surfaces [5,16,47,48,68], whereas the density functional theory, consistently underestimates the band gap of complex oxide materials. From another side, it is well known that the Hartree–Fock method considerably overestimates the band gap of complex oxide materials. The B3LYP-calculated bulk band gap for ReO_3 at the Γ-point is equal to 5.76 eV (Table 4). To the best of our knowledge, there are no reported experimental data for the ReO_3 bulk band gap at the Γ-point. The calculated optical band gap for $BaZrO_3$ at the Γ-point (4.93 eV) is only underestimated by 6.98% regarding the experimental value of 5.3 eV [69]. The ab initio calculated optical band gaps at the Γ-point for $SrZrO_3$, $PbZrO_3$ and $CaZrO_3$ perovskite cubic phases are 5.31, 5.63 and 5.40 eV, respectively. Unfortunately, it is not possible to compare the ab initio calculation results for the band gaps at the Γ-point for $SrZrO_3$, $PbZrO_3$ and $CaZrO_3$ perovskites with experimental results, since there are, currently, no reports of the band gaps of $SrZrO_3$, $PbZrO_3$ and $CaZrO_3$ perovskite cubic phases in the literature.

Table 4. B3LYP or B3PW calculated ReO_3, $SrZrO_3$, $BaZrO_3$, $PbZrO_3$ and $CaZrO_3$ bulk band gaps at the Γ–Γ point for the cubic phase. The ab initio calculation results are compared with the available experimental data.

Material	Method	Optical Band Gap at Γ–Γ Point	
		Ab initio Data	Experimental Data
ReO_3	B3LYP	5.76	No data for Γ–Γ band gap
$SrZrO_3$	B3LYP	5.31	No data for cubic phase
$BaZrO_3$	B3PW	4.93	5.3 [69]
$PbZrO_3$	B3LYP	5.63	No data for cubic phase
$CaZrO_3$	B3LYP	5.40	No data for cubic phase

3.2. *Ab Initio Calculations of ReO_3, $SrZrO_3$, $BaZrO_3$, $PbZrO_3$ and $CaZrO_3$ (001) Surfaces*

B3LYP or B3PW ab initio calculations for the upper three-layer atom relaxation for the neutral ZrO_2-terminated $SrZrO_3$, $BaZrO_3$, $PbZrO_3$ and $CaZrO_3$ as well as polar ReO_2-terminated ReO_3 (001) surfaces (Table 5) were performed. It is worth noting that the ReO_3 material has the cubic ABO_3 perovskite structure and symmetry with the space group number 221, but with the only difference being the A atom vacancy (Figure 2). For the cases of $SrZrO_3$, $BaZrO_3$, $PbZrO_3$ and $CaZrO_3$ perovskite ZrO_2-terminated as well as ReO_3 crystal ReO_2-terminated (001) surfaces, according to the ab initio calculations, all upper-layer atoms relax towards the bulk (Table 5). The ReO_2-terminated ReO_3 (001) surface upper-layer Re atom displacement magnitude (3.19% of a_0) is slightly larger than the ab initio calculated ABO_3 perovskite ZrO_2-terminated (001) surface Zr atom relaxation magnitudes, which are in the range of 1.30% of a_0 for the $CaZrO_3$ to 2.37% of a_0 for the $PbZrO_3$ perovskite (Table 5). In contrast, all $SrZrO_3$, $BaZrO_3$, $PbZrO_3$ and $CaZrO_3$ perovskite second-layer ZrO_2-terminated (001) surface atoms relax in the outward direction. The only exception to this systematic trend is the second-layer ReO_2-terminated ReO_3 (001) surface O atom inward relaxation towards the bulk; however, this has a small relaxation magnitude, equal to −0.32% of a_0. All the ab initio calculated third-layer atoms for the ZrO_2-terminated $SrZrO_3$, $BaZrO_3$, $PbZrO_3$ and $CaZrO_3$ as well as ReO_2-terminated ReO_3 (001) surfaces, again, as in the case of the upper-layer atoms, relax inwards, towards the crystal bulk (Table 5). Nevertheless, the relaxation magnitudes of all first-layer atoms for the ZrO_2-terminated $SrZrO_3$, $BaZrO_3$, $PbZrO_3$ and $CaZrO_3$ perovskite as well as ReO_2-terminated ReO_3 (001) surfaces are much larger than the relevant relaxation magnitudes of the respective third-layer atoms (Table 5).

To compare ab initio calculation results for ReO_3, $SrZrO_3$, $BaZrO_3$, $PbZrO_3$ and $CaZrO_3$ (001) surfaces with the available experimental results, the calculated surface rumplings s (the relative displacement of oxygen with respect to the metal in the upper surface layer) as well as the changes in interlayer distances, Δd_{12} and Δd_{23}, are shown in Table 6. The calculations of the ReO_3, $SrZrO_3$, $BaZrO_3$, $PbZrO_3$ and $CaZrO_3$ (001) surface interlayer distances rely on the positions of the metal ions (Figure 1), which are well known to be much stronger electron scatterers than oxygen ions [70]. As can be seen

from Table 6, all the calculated ZrO_2-terminated $SrZrO_3$, $BaZrO_3$, $PbZrO_3$ and $CaZrO_3$ (001) surfaces show the reduction of the interlayer distance Δd_{12} and expansion of Δd_{23}. For all ZrO_2-terminated $SrZrO_3$, $BaZrO_3$, $PbZrO_3$ and $CaZrO_3$ (001) surfaces, the reduction in the interlayer distance, Δd_{12}, is larger than the expansion of the respective interlayer distance, Δd_{23}. The ab initio calculated surface rumpling, s, is positive and largest between all calculated surface rumplings (+2.02) for the ReO_2-terminated ReO_3 (001) surface. The calculated surface rumplings, s, for the ZrO_2-terminated $BaZrO_3$ and $PbZrO_3$ (001) surfaces (+0.09 and +0.38, respectively) are also positive, but much smaller than for the ReO_2-terminated ReO_3 (001) surface (+2.02). In contrast, the calculated surface rumplings, s, for the ZrO_2-terminated $SrZrO_3$ and $CaZrO_3$ (001) surfaces are negative (−0.72 and −1.01, respectively).

Table 5. ReO_3, $SrZrO_3$, $BaZrO_3$, $PbZrO_3$ and $CaZrO_3$ upper three-layer atom relaxation (in percent of the crystal bulk lattice constant) for the BO_2-terminated (001) surfaces calculated by the B3LYP exchange–correlation functional for ReO_3, $SrZrO_3$, $PbZrO_3$ and $CaZrO_3$ perovskites as well as by the B3PW method for $BaZrO_3$.

Surfaces, (001)		**ReO_3**	**$SrZrO_3$**	**$BaZrO_3$**	**$PbZrO_3$**	**$CaZrO_3$**
Layer	**Ion**	**ReO_2-t.**	**ZrO_2-t.**	**ZrO_2-t.**	**ZrO_2-t.**	**ZrO_2-t.**
1	B	−3.19	−1.38	−1.79	−2.37	−1.30
	O	−1.17	−2.10	−1.70	−1.99	−2.31
2	A	Absent	+2.81	+1.94	+4.36	+4.23
	O	−0.32	+0.91	+0.85	+1.04	+1.25
3	B	−0.17	−0.04	−0.03	−0.47	−0.05
	O	−0.11	−0.05	0.00	−0.28	−0.09

Table 6. B3PW and B3LYP calculated surface rumplings, s, as well as relative displacements, Δd_{ij}, between the 3 near-surface planes for the BO_2-terminated ReO_3, $SrZrO_3$, $BaZrO_3$, $PbZrO_3$ and $CaZrO_3$ (001) surfaces as a percent of the bulk crystal lattice constant.

Material	**Method**	**BO_2-Terminated (001) Surface**		
		s	Δd_{12}	Δd_{23}
ReO_3	B3LYP	+2.02	–	–
$SrZrO_3$	B3LYP	−0.72	−4.19	+2.85
$BaZrO_3$	B3PW	+0.09	−3.73	+1.97
$PbZrO_3$	B3LYP	+0.38	−6.73	+4.83
$CaZrO_3$	B3LYP	−1.01	−5.53	+4.28

Unfortunately, to the best of our knowledge, there are no experimental data available for the ReO_3, $SrZrO_3$, $BaZrO_3$, $PbZrO_3$ and $CaZrO_3$ (001) surface rumpling, s, as well as interlayer distances, Δd_{12} and Δd_{23}. However, such experimental data exist for the related ABO_3 perovskite, $SrTiO_3$ (Table 7). To compare the calculated and experimental $SrTiO_3$ (001) surface structures, the calculated surface rumpling, s, as well as the changes in interlayer distances, Δd_{ij}, are detailed in Table 7. From Table 7, it can be seen that the agreement is fairly good for all theoretical calculation methods, which all give the same sign for the surface rumpling, s, as well as the changes in the interlayer distances, Δd_{ij}. For example, the calculated surface rumpling, s, for the SrO-terminated surface is much larger than for the TiO_2-terminated $SrTiO_3$ (001) surface for all theoretical methods [25,71–75]. From Table 7, it can be seen that both the calculated SrO and TiO_2-terminated $SrTiO_3$ (001) surfaces always exhibit a reduction in the interlayer distance, Δd_{12} and an expansion of Δd_{23}. The theoretically calculated surface rumpling amplitudes, s, for both $SrTiO_3$ (001) surface terminations are in fair agreement with the LEED [70], RHEED [76], MEIS [77] and SXRD [78] experiments (Table 7). Nevertheless, the calculated changes in interlayer distances disagree with the LEED experiments [70] for the TiO_2-terminated $SrTiO_3$ (001) surface, which show an increase in Δd_{12} and reduction in Δd_{23} (Table 7). In contrast, all ab initio as well as classical shell model calculations show a reduction in the interlayer distance, Δd_{12} and an expansion

of Δd_{23} (Table 7). Nevertheless, as can be seen from Table 7, unfortunately, the different experiments contradict each other with respect to the sign of Δd_{12} and Δd_{23} for the SrO-terminated $SrTiO_3$ (001) surface and for the sign of Δd_{23} for the TiO_2-terminated $SrTiO_3$ (001) surface (Table 7).

Table 7. Calculated and experimental surface rumpling s and relative displacements Δd_{ij} (in percent of the bulk lattice constant) for the upper-three surface layers of SrO and TiO_2-terminated $SrTiO_3$ (001) slabs.

$SrTiO_3$	SrO-Terminated $SrTiO_3$ (001) Surf.			TiO_2-Terminated $SrTiO_3$ (001) Surf.		
	s	Δd_{12}	Δd_{23}	s	Δd_{12}	Δd_{23}
Ab initio [25,71]	5.66	−6.58	1.75	2.12	−5.79	3.55
Shell model [72]	8.2	−8.6	3.0	1.2	−6.4	4.0
HF-LYP [73]	3.8	−4.3	1.3	1.2	−4.9	2.2
Ab initio [74]	5.8	−6.9	2.4	1.8	−5.9	3.2
Ab initio [75]	7.7	−8.6	3.3	1.5	−6.4	4.9
LEED exp. [70]	4.1 ± 2	−5 ± 1	2 ± 1	2.1 ± 2	1 ± 1	−1 ± 1
RHEED exp. [76]	4.1	2.6	1.3	2.6	1.8	1.3
MEIS exp. [77]				1.5 ± 0.2	0.5 ± 0.2	
SXRD exp. [78]	1.3 ± 12.1	−0.3 ± 3.6	−6.7 ± 2.8	12.8 ± 8.5	0.3 ± 1	

The ab initio calculated atomic displacements, the Mulliken static charges as well as bond populations between nearest atoms are reported in Table 8. The most important effect, as can be seen from Table 8, is strengthening of the Zr–O chemical bond near the ZrO_2-terminated $SrZrO_3$, $BaZrO_3$, $PbZrO_3$ and $CaZrO_3$ (001) surface in comparison to the bulk [79–82]. In contrast, for the ReO_2-terminated ReO_3 (001) surface, the chemical bond population between the Re and O atoms in the upper surface layer 0.170e (Table 8) is slightly smaller than the Re–O chemical bond population in the ReO_3 bulk (0.212e). Nevertheless, the chemical bond population between the upper-layer Re atom and the second-layer O atom (0.262e) for the ReO_2-terminated ReO_3 (001) surface is considerably larger than the Re–O chemical bond population in the ReO_3 crystal bulk (0.212e). It is worth noticing, that the Re and O effective charges in the ReO_3 crystal bulk (+2.382e for Re and −0.794e for O) are much smaller than those expected in the ionic model (+6e for Re and −2e for O). Moreover, the Re–O chemical bond in the ReO_3 bulk is considerably populated (+0.212e). It is interesting to note that the Re–O chemical bond population for the ReO_2-terminated ReO_3 (001) surface third layer (+0.208e) (Table 8) is already highly similar to the Re–O chemical bond population in the ReO_3 bulk matrix (0.212e). The Re effective charge in the ReO_2-terminated ReO_3 (001) surface third layer (+2.341e) is almost as high as the Re effective charge value (+2.382e) in the ReO_3 bulk crystal. In contrast, the Re effective charge on the ReO_2-terminated ReO_3 (001) surface upper layer, where the surface effect is strong, (+2.258e) is much smaller than the Re effective charge in the ReO_3 crystal bulk (+2.382e).

As can be seen from the ab initio calculation results, detailed in Table 9, the Zr–O chemical bond populations for all four calculated perovskites $SrZrO_3$, $BaZrO_3$, $PbZrO_3$ and $CaZrO_3$ are larger near their ZrO_2-terminated (001) surfaces than in the bulk. However, the opposite is true for the ReO_3 crystal. The Re–O chemical bond population in the ReO_3 bulk (0.212e) is larger than it is near the ReO_2-terminated ReO_3 (001) surface (0.170e). However, it is worth noting that the Re–O chemical bond population between the ReO_2-terminated (001) surface upper-layer Re atom and the second-layer O atom (0.262e) is considerably larger than the Re–O chemical bond population in the ReO_3 crystal bulk (0.212e).

The, by means of the hybrid exchange–correlation functionals, calculated bulk band gaps at the Γ–Γ point for ReO_3, $SrZrO_3$, $BaZrO_3$, $PbZrO_3$ and $CaZrO_3$ crystals are equal to 5.76, 5.31, 4.93, 5.63 and 5.40 eV, respectively (Table 10). In most cases, there are no experimental data available for the ReO_3, $SrZrO_3$, $BaZrO_3$, $PbZrO_3$ and $CaZrO_3$ bulk band gaps in the cubic phase. However, the calculated $BaZrO_3$ band gap at the Γ–Γ point (4.93 eV) is in fair agreement with the experimental data (5.3 eV) [69]. According to the performed ab initio calculations, the systematic trend is reduction of the ReO_3, $SrZrO_3$,

$BaZrO_3$, $PbZrO_3$ and $CaZrO_3$ bulk band gaps near their ReO_2 or ZrO_2-terminated (001) surfaces, respectively. Namely, the calculated band gap values at the Γ–Γ point for ReO_2-terminated ReO_3 and ZrO_2-terminated $SrZrO_3$, $BaZrO_3$, $PbZrO_3$ and $CaZrO_3$ terminated (001) surfaces of 0.22, 4.91, 4.48, 4.60 and 5.22 eV, respectively, were always smaller with respect to the bulk band gap value (Table 10).

Table 8. Ab initio calculated absolute magnitudes of atomic shifts *D* (in Å), the effective atomic charges Q (in *e*) and nearest atom Me–O bond populations *P* (in *e*) for the ReO_2 and ZrO_2-terminated ReO_3, $SrZrO_3$, $BaZrO_3$, $PbZrO_3$ and $CaZrO_3$ (001) surfaces.

ReO_2 and ZrO_2-Term. (001) Surfaces			**ReO_3**	**SZO**	**BZO**	**PZO**	**CZO**
Layer	**Property**	**Ion**	**ReO_2**	**ZrO_2**	**ZrO_2**	**ZrO_2**	**ZrO_2**
1	*D*	B	−0.120	−0.058	−0.076	−0.100	−0.054
	Q		+2.258	+2.196	+2.173	+2.165	+2.172
	P		+0.170	+0.114	+0.132	+0.116	+0.102
	D	O	−0.044	−0.088	−0.72	−0.084	−0.096
	Q		−0.933	−1.277	−1.239	−1.171	−1.258
	P		−0.012	−0.002	−0.018	+0.046	+0.018
2	*D*	A	–	+0.118	+0.082	+0.184	+0.176
	Q		–	+1.869	+1.797	+1.357	+1.772
	P		–	+0.002	−0.010	+0.022	+0.012
	D	O	−0.012	+0.038	+0.036	+0.044	+0.052
	Q		−0.742	−1.287	−1.273	−1.103	−1.235
	P		+0.214	+0.094	+0.106	+0.098	+0.090
3	*D*	B	−0.006	−0.002	−0.001	−0.020	−0.002
	Q		+2.341	+2.172	+2.133	+2.116	+2.14
	P		+0.208	+0.102	+0.116	+0.124	+0.098
	D	O	−0.004	−0.002	0.000	−0.012	−0.004
	Q		−0.801	−1.331	−1.30	−1.148	−1.286
	P		−0.036	+0.002	−0.012	+0.036	+0.014

Table 9. Ab initio calculated B–O chemical bond populations for ReO_3, $SrZrO_3$, $BaZrO_3$, $PbZrO_3$ and $CaZrO_3$ bulk as well as for BO_2-terminated (001) surfaces (in *e*).

Material	**Method**	**B–O Chemical Bond Populations**	
		Bulk	**BO_2-Termin., (001)**
ReO_3	B3LYP	0.212	0.170
$SrZrO_3$	B3LYP	0.092	0.114
$BaZrO_3$	B3PW	0.108	0.132
$PbZrO_3$	BLYP	0.106	0.116
$CaZrO_3$	B3LYP	0.086	0.102

Table 10. Ab initio calculated optical band gaps at the Γ–Γ point for ReO_3, $SrZrO_3$, $BaZrO_3$, $PbZrO_3$ and $CaZrO_3$ bulk as well as their ReO_2 or ZrO_2-terminated (001) surfaces.

Material	**Method**	**Band Gap at Γ–Γ Point**	
		Bulk	**BO_2-Termin. (001)**
ReO_3	B3LYP	5.76	0.22
$SrZrO_3$	B3LYP	5.31	4.91
$BaZrO_3$	B3PW	4.93	4.48
$PbZrO_3$	B3LYP	5.63	4.60
$CaZrO_3$	B3LYP	5.40	5.22

4. Conclusions

For the ab initio calculated ReO_2-terminated ReO_3 as well as ZrO_2-terminated $SrZrO_3$, $BaZrO_3$, $PbZrO_3$ and $CaZrO_3$ (001) surfaces, the systematic trend was that all upper-layer surface atoms relaxed inwards, towards the bulk, all second-layer surface atoms relaxed upwards, and again, all third-layer surface atoms relaxed inwards. As a result of the performed relaxation, all five material surfaces exhibited a reduction in the interlayer distance, Δd_{12} and expansion of Δd_{23}.

For all the ab initio calculated materials, the changes in the interlayer distances between the first and second layer were larger than the respective changes in the interlayer distances between the second and third layer.

According to the performed ab initio calculations, the $SrZrO_3$, $BaZrO_3$, $PbZrO_3$ and $CaZrO_3$ perovskite BO_2-terminated as well as ReO_2-terminated ReO_3 (001) surface band gaps were always smaller with respect to their bulk band gap values.

The Zr–O chemical bond population in $SrZrO_3$, $BaZrO_3$, $PbZrO_3$ and $CaZrO_3$ perovskite bulk was always smaller than that near the ZrO_2-terminated (001) surface. In contrast, the Re–O chemical bond population in the ReO_3 bulk (0.212*e*) was larger than that near the ReO_2-terminated ReO_3 (001) surface (0.170*e*). The Re–O chemical bond population between the Re atom located on the ReO_2-terminated ReO_3 (001) surface upper layer as well as the O atom located on the ReO_2-terminated ReO_3 (001) surface second layer was the largest (0.262*e*).

Author Contributions: All authors equally contributed to the performed ab initio calculations as well as to the preparation of the manuscript. Namely, mostly R.I.E. and A.I.P. wrote the Introduction. Mostly J.P., J.G. and R.J. wrote the section Computational Method. All authors equally wrote the sections Numeric Results and Conclusions. All authors have read and agreed to the published version of the manuscript.

Funding: This research was funded by Latvian Government ERAF Grant number 1.1.1.1/18/A/073.

Acknowledgments: We greatly acknowledge the financial support via the ERAF Project No. 1.1.1.1/18/A/073.

Conflicts of Interest: The authors declare no conflict of interests.

References

1. Mastrikov, Y.A.; Merkle, R.; Kotomin, E.A.; Kuklja, M.M.; Maier, J. Surface termination effects on the oxygen reduction reaction rate at fuel cell cathodes. *J. Mater. Chem. A* **1998**, *6*, 11929–11940. [CrossRef]
2. Enterkin, J.A.; Subramanian, A.K.; Russell, B.C.; Castell, M.R.; Poeppelmeier, K.R.; Marks, L.D. A homologous series of structures on the surface of $SrTiO_3$ (110). *Nat. Mater.* **2010**, *9*, 245–248. [CrossRef] [PubMed]
3. Piskunov, S.; Eglitis, R.I. First principles hybrid DFT calculations of $BaTiO_3/SrTiO_3$ (001) interface. *Solid State Ion.* **2015**, *274*, 29–33. [CrossRef]
4. Saeed, S.W.; Norby, T.; Bjornheim, T.S. Charge-Carrier enrichment at $BaZrO_3/SrTiO_3$ interfaces. *J. Phys. Chem. C* **2019**, *123*, 20808–20816. [CrossRef]
5. Eglitis, R.I. Comparative ab initio calculations of $SrTiO_3$ and $CaTiO_3$ polar (111) surfaces. *Phys. Status Solidi B* **2015**, *252*, 635–642. [CrossRef]
6. Zhao, X.H.; Selloni, A. Structure and stability of $NaTaO_3$ (001) and $KTaO_3$ (001) surfaces. *Phys. Rev. Mater.* **2019**, *3*, 015801. [CrossRef]
7. Eglitis, R.I.; Kleperis, J.; Purans, J.; Popov, A.I.; Jia, R. Ab initio calculations of $CaZrO_3$ (011) surfaces: Systematic trends in polar (011) surface calculations of ABO_3 perovskites. *J. Mater. Sci.* **2020**, *55*, 203–217. [CrossRef]
8. Watanabe, Y. Ferroelectricity of stress-free and strained pure $SrTiO_3$ revealed by ab initio calculations with hybrid and density functionals. *Phys. Rev. B* **2019**, *99*, 064107. [CrossRef]
9. Piskunov, S.; Eglitis, R.I. Comparative ab initio calculations of $SrTiO_3/BaTiO_3$ and $SrZrO_3/PbZrO_3$ (001) heterostructures. *Nucl. Instrum. Methods B* **2016**, *374*, 20–23. [CrossRef]
10. Meng, J.; Lan, Z.Y.; Lin, Q.Y.; Chen, T.; Chen, X.; Wei, X.; Lu, Y.H.; Li, J.X.; Zhang, Z. Cubic-like $BaZrO_3$ nanocrystals with exposed {001}/{011} facets and tuned electronic band structure for enhanced photocatalytic hydrogen production. *J. Mater. Sci.* **2019**, *54*, 1967–1976. [CrossRef]

11. Eglitis, R.I. First-principles calculations of $BaZrO_3$ (001) and (011) surfaces. *J. Phys. Condens. Matter* **2007**, *19*, 356004. [CrossRef]
12. Sambrano, J.R.; Longo, V.M.; Longo, E.; Taft, C.A. Electronic and structural properties of the (001) $SrZrO_3$ surface. *J. Mol. Struct. THEOCHEM* **2007**, *813*, 49–56. [CrossRef]
13. Kim, J.S.; Yang, J.H.; Kim, B.K.; Kim, Y.C. Proton conduction at BaO-terminated (001) $BaZrO_3$ surface using density functional theory. *Solid State Ion.* **2015**, *275*, 19–22. [CrossRef]
14. Eglitis, R.I.; Rohlfing, M. First-principles calculations of the atomic and electronic structure of $SrZrO_3$ and $PbZrO_3$ (001) and (011) surfaces. *J. Phys. Condens. Matter* **2010**, *22*, 415901. [CrossRef] [PubMed]
15. Brik, M.G.; Ma, C.G.; Krasnenko, V. First-principles calculations of the structural and electronic properties of the cubic $CaZrO_3$ (001) surfaces. *Surf. Sci.* **2013**, *608*, 146–153. [CrossRef]
16. Eglitis, R.I.; Popov, A.I. Systematic trends in (001) surface ab initio calculations of ABO_3 perovskites. *J. Saudi Chem. Soc.* **2018**, *22*, 459–468. [CrossRef]
17. Guo, X.; Ge, J.; Ponchel, F.; Remiens, D.; Chen, Y.; Dong, X.; Wang, G. Effect of Sn substitution on the energy storage properties of high (001)-oriented $PbZrO_3$ thin films. *Thin Solid Films* **2017**, *632*, 93–96. [CrossRef]
18. Kotomin, E.A.; Piskunov, S.; Zhukovskii, Y.F.; Eglitis, R.I.; Gopejenko, A.; Ellis, D.E. The electronic properties of an oxygen vacancy at ZrO_2-terminated (001) surfaces of a cubic $PbZrO_3$: Computer simulations from the first principles. *Phys. Chem. Chem. Phys.* **2008**, *10*, 4258–4263. [CrossRef]
19. Sung, H.J.; Mochizuki, Y.; Oba, F. Surface reconstruction and band alignment of nonmetallic A(II)B(IV)O_3 perovskites. *Phys. Rev. Mater.* **2020**, *4*, 044606. [CrossRef]
20. Eglitis, R.I.; Piskunov, S. First principles calculations of $SrZrO_3$ bulk and ZrO_2-terminated (001) surface *F* centers. *Comput. Condens. Matter* **2016**, *7*, 1–6. [CrossRef]
21. Nguyen, M.D.; Trinh, T.T.; Dang, H.T.; Hung, N.V. Understanding the effects of electric-field-induced phase transition and polarization loop behavior on the energy storage performance of antiferroelectric $PbZrO_3$ thin films. *Thin Solid Films* **2020**, *697*, 137794. [CrossRef]
22. Eglitis, R.I.; Purans, J.; Popov, A.I.; Jia, R. Systematic trends in $YAlO_3$, $SrTiO_3$, $BaTiO_3$, $BaZrO_3$ (001) and (111) surface ab initio calculations. *Int. J. Mod. Phys. B* **2019**, *33*, 1950390. [CrossRef]
23. Hwang, H.Y.; Iwasa, Y.; Kawasaki, M.; Keimer, B.; Nagaosa, N.; Tokura, Y. Emergent phenomena at oxide interfaces. *Nat. Mater.* **2012**, *11*, 103–113. [CrossRef] [PubMed]
24. Mueller, D.N.; Machala, M.L.; Bluhm, H.; Chuech, W.C. Redox activity of surface oxygen anions in oxygen-deficient perovskite oxides during electrochemical reactions. *Nat. Commun.* **2015**, *6*, 6097. [CrossRef]
25. Eglitis, R.I.; Vanderbilt, D. First-principles calculations of atomic and electronic structure of $SrTiO_3$ (001) and (011) surfaces. *Phys. Rev. B* **2008**, *77*, 195408. [CrossRef]
26. Nahas, Y.; Akbarzadeh, A.; Prokharenko, S.; Prosandeev, S.; Walter, R.; Kornev, I.; Iniguez, J.; Bellaiche, L. Microscopic origins of the large piezoelectricity of leadfree (Ba,Ca)(Zr,Ti)O_3. *Nat. Commun.* **2017**, *8*, 15944. [CrossRef]
27. Jia, W.; Vikhnin, V.S.; Liu, H.; Kapphan, S.; Eglitis, R.; Usvyat, D. Critical effects in optical response due to charge transfer vibronic excitions and their structure in perovskite-like systems. *J. Lumin.* **1999**, *83*, 109–113. [CrossRef]
28. Ji, Q.; Bi, L.; Zhang, J.; Cao, H.; Zhao, X.S. The role of oxygen vacancies of ABO_3 perovskite oxides in the oxygen reduction reaction. *Energy Environ. Sci.* **2020**, *13*, 1408–1428. [CrossRef]
29. Wrana, D.; Rodenbucher, C.; Belza, W.; Szot, K.; Krok, F. In situ study of redox processes on the surface of $SrTiO_3$ single crystals. *Appl. Surf. Sci.* **2018**, *432*, 46–52. [CrossRef]
30. Wojtyniak, M.; Balin, K.; Szade, J.; Szot, K. Inhomogeneity and segregation effect in the surface layer of Fe-doped $SrTiO_3$ single crystals. *Crystals* **2020**, *10*, 33. [CrossRef]
31. Rodenbucher, C.; Meuffels, P.; Speier, W.; Ermich, M.; Wrana, D.; Krok, F.; Szot, K. Stability and decomposition of perovskite-type titanates upon high temperature reduction. *Phys. Status Solidi Rapid Res. Lett.* **2017**, *11*, 1700222. [CrossRef]
32. Eglitis, R.; Kruchinin, S.P. Ab initio calculations of ABO_3 perovskite (001), (011) and (111) nano-surfaces, interfaces and defects. *Mod. Phys. Lett. B* **2020**, *34*, 2040057. [CrossRef]
33. Evarestov, R.A.; Kalinko, A.; Kuzmin, A.; Losev, M.; Purans, J. First-principles LCAO calculations on 5d transition metal oxides: Electronic and phonon properties. *Integr. Ferroelectr.* **2009**, *108*, 1–10. [CrossRef]
34. Ling, S.; Mei, D.; Gutowski, M. Reactivity of hydrogen and methanol on (001) surfaces of WO_3, ReO_3, WO_3/ReO_3 and ReO_3/WO_3. *Catal. Today* **2011**, *165*, 41–48. [CrossRef]

35. Tsukada, M.; Tsukada, N.; Minami, F. Theory of the electronic structure of ReO_3 (001) surface and the surface oxygen vacancy. *J. Phys. Soc. Jpn.* **1980**, *49*, 1115–1122. [CrossRef]
36. Ge, Q.; Gutowski, M. A comparative study of methanol adsorption and dissociation over WO_3 (001) and ReO_3 (001). *Top. Catal.* **2015**, *58*, 655–664. [CrossRef]
37. Evans, H.A.; Wu, Y.; Seshadri, R.; Cheetham, A.K. Perovskite-related ReO_3-type structures. *Nat. Rev. Mater.* **2020**, *5*, 196–213. [CrossRef]
38. Bashian, N.H.; Zhou, S.; Zuba, M.; Ganose, A.M.; Stiles, J.W.; Ee, A.; Ashby, D.S.; Scanlon, D.O.; Piper, L.F.J.; Dunn, B.; et al. Correlated polyhedral rotation in the absence of polarons during electrochemical insertion of lithium in ReO_3. *ACS Energy Lett.* **2018**, *3*, 2513–2519. [CrossRef]
39. Ceder, G.; Chiang, Y.M.; Sadoway, D.R.; Aydinol, M.K.; Jang, Y.I.; Huang, B. Identification of cathode materials for lithium batteries guided by first-principles calculations. *Nature* **1998**, *392*, 694–696. [CrossRef]
40. Ceder, G. Predicting properties from scratch. *Science* **1998**, *280*, 1099–1100. [CrossRef]
41. Eglitis, R.I.; Borstel, G. Towards a practical rechargeable 5 V Li ion battery. *Phys. Status Solidi A* **2005**, *202*, R13–R15. [CrossRef]
42. Eglitis, R. Ab initio calculations of $Li_2(Co,Mn)O_8$ solid solutions for rechargeable batteries. *Int. J. Mod. Phys. B* **2019**, *33*, 1950151. [CrossRef]
43. Becke, A.D. Density-functional thermochemistry. III. The role of exact exchange. *J. Chem. Phys.* **1993**, *98*, 5648–5652. [CrossRef]
44. Lee, C.; Yang, W.; Parr, R.G. Development of the Colle-Salvetti correlation-energy formula into a functional of the electron density. *Phys. Rev. B* **1988**, *37*, 785–789. [CrossRef] [PubMed]
45. Saunders, V.R.; Dovesi, R.; Roetti, C.; Causa, N.; Harrison, N.M.; Orlando, R.; Zicovich-Wilson, C.M. *CRYSTAL-2009 User Manual*; University of Torino: Torino, Italy, 2009.
46. Piskunov, S.; Heifets, E.; Eglitis, R.I.; Borstel, G. Bulk properties and electronic structure of $SrTiO_3$, $BaTiO_3$, $PbTiO_3$ perovskites: An ab initio HF/DFT study. *Comput. Mater. Sci.* **2004**, *29*, 165–178. [CrossRef]
47. Shi, H.; Eglitis, R.I.; Borstel, G. Ab initio calculations of the CaF_2 electronic structure and F centers. *Phys. Rev. B* **2005**, *72*, 045109. [CrossRef]
48. Vassilyeva, A.F.; Eglitis, R.I.; Kotomin, E.A.; Dauletbekova, A.K. Ab initio calculations of MgF_2 (001) and (011) surface structure. *Phys. B Condens. Matter* **2010**, *405*, 2125–2127. [CrossRef]
49. van Benthem, K.; Elsasser, C.; French, R.H. Bulk electronic structure of $SrTiO_3$: Experiment and theory. *J. Appl. Phys.* **2001**, *90*, 6156–6164. [CrossRef]
50. Rubloff, G.W. Far-Ultraviolet Reflectance Spectra and the electronic structure of ionic crystals. *Phys. Rev. B* **1972**, *5*, 662–684. [CrossRef]
51. Thomas, J.; Stephan, G.; Lemonnier, J.C.; Nisar, M.; Robin, S. Optical anisotropy of MgF_2 in its UV absorption region. *Phys. Status Solidi B* **1973**, *56*, 163–170. [CrossRef]
52. Lisitsyn, V.M.; Lisitsyna, L.A.; Popov, A.I.; Kotomin, E.A.; Abuova, F.U.; Akilbekov, A.; Maier, J. Stabilization of primary mobile radiation defects in MgF_2 crystals. *Nucl. Instrum. Methods B* **2016**, *374*, 24–28. [CrossRef]
53. Eglitis, R.I. Ab initio calculations of the atomic and electronic structure of $BaZrO_3$ (111) surfaces. *Solid State Ion.* **2013**, *230*, 43–47. [CrossRef]
54. Eglitis, R.I. Comparative first-principles calculations of $SrTiO_3$, $BaTiO_3$, $PbTiO_3$ and $CaTiO_3$ (001), (011) and (111) surfaces. *Ferroelectrics* **2015**, *483*, 53–67. [CrossRef]
55. Liu, W.; Wang, C.; Cui, J.; Man, Z.Y. Ab initio calculations of the $CaTiO_3$ (111) polar surfaces. *Solid State Commun.* **2009**, *149*, 1871–1876. [CrossRef]
56. Pojani, A.; Finocchi, F.; Noguera, C. Polarity of the $SrTiO_3$ (111) and (110) surfaces. *Surf. Sci.* **1999**, *442*, 179–198. [CrossRef]
57. Pojani, A.; Finocchi, F.; Noguera, C. A theoretical study of the unreconstructed polar (111) face of $SrTiO_3$. *Appl. Surf. Sci.* **1999**, *142*, 177–181. [CrossRef]
58. Noguera, C. Polar oxide surfaces. *J. Phys. Condens. Matter* **2000**, *12*, R367–R410. [CrossRef]
59. Tasker, P.W. The stability of ionic crystal surfaces. *J. Phys. C Solid State Phys.* **1979**, *12*, 4977–4984. [CrossRef]
60. Mayer, I. Bond order and valence: Relations to Mulliken's population analysis. *Int. J. Quantum Chem.* **1984**, *26*, 151–154. [CrossRef]
61. Bochicchio, R.C.; Reale, H.F. On the nature of crystalline bonding-extension of statistical population analysis to 2-dimensional and 3-dimensional crystalline systems. *J. Phys. B* **1993**, *26*, 4871–4883. [CrossRef]

62. Eglitis, R.I. Ab initio calculations of $SrTiO_3$, $BaTiO_3$, $PbTiO_3$, $CaTiO_3$, $SrZrO_3$, $PbZrO_3$ and $BaZrO_3$ (001), (011) and (111) surfaces as well as *F* centers, polarons, KTN solid solutions and Nb impurities therein. *Int. J. Mod. Phys. B* **2014**, *28*, 1430009. [CrossRef]
63. Schirber, J.E.; Morosin, B. "Compressibility Collapse" transition in ReO_3. *Phys. Rev. Lett.* **1979**, *42*, 1485–1487. [CrossRef]
64. Kennedy, B.J.; Howard, C.J.; Chakoumakos, B.C. High-temperature phase transitions in $SrZrO_3$. *Phys. Rev. B* **1999**, *59*, 4023–4027. [CrossRef]
65. Mathews, M.D.; Mirza, E.B.; Momin, A.C. High-temperature X-ray diffractometric studies of $CaZrO_3$, $SrZrO_3$ and $BaZrO_3$. *J. Mater. Sci. Lett.* **1991**, *10*, 305–306. [CrossRef]
66. Aoyagi, S.; Kuroiwa, Y.; Sawada, A.; Tanaka, H.; Nishibori, E.; Takata, M.; Sakata, M. Direct observation of covalency between O and disordered Pb in cubic $PbZrO_3$. *J. Phys. Soc. Jpn.* **2002**, *71*, 2353–2356. [CrossRef]
67. Eglitis, R.I. Theoretical modelling of the energy surface (001) and topology of $CaZrO_3$ perovskite. *Ferroelectrics* **2008**, *483*, 75–85. [CrossRef]
68. Shi, H.; Chang, L.; Jia, R.; Eglitis, R.I. Ab initio calculations of the charge transfer and aggregation of F centers in CaF_2. *J. Phys. Chem. C* **2012**, *116*, 4832–4839. [CrossRef]
69. Robertson, J. Band offsets of wide-band-gap oxides and implications for future electronic devices. *J. Vac. Sci. Technol. B* **2000**, *18*, 1785–1791. [CrossRef]
70. Bickel, N.; Schmidt, G.; Heinz, K.; Muller, K. Ferroelectric relaxation of the $SrTiO_3$ (100) surface. *Phys. Rev. Lett.* **1989**, *62*, 2009–2011. [CrossRef]
71. Piskunov, S.; Kotomin, E.A.; Heifets, E.; Maier, J.; Eglitis, R.I.; Borstel, G. Hybrid DFT calculations of the atomic and electronic structure for ABO_3 perovskite (001) surfaces. *Surf. Sci.* **2005**, *575*, 75–88. [CrossRef]
72. Heifets, E.; Kotomin, E.A.; Maier, J. Semi-empirical simulations of surface relaxation for perovskite titanates. *Surf. Sci.* **2000**, *462*, 19–35. [CrossRef]
73. Heifets, E.; Eglitis, R.I.; Kotomin, E.A.; Maier, J.; Borstel, G. Ab initio modeling of surface structure for $SrTiO_3$ perovskite. *Phys. Rev. B* **2001**, *64*, 235417. [CrossRef]
74. Padilla, J.; Vanderbilt, D. Ab initio study of $SrTiO_3$ surfaces. *Surf. Sci.* **1998**, *418*, 64–70. [CrossRef]
75. Cheng, C.; Kunc, K.; Lee, M.H. Structural relaxation and longitudinal dipole moment of $SrTiO_3$ (001) (1×1) surfaces. *Phys. Rev. B* **2000**, *62*, 10409. [CrossRef]
76. Hikita, T.; Hanada, T.; Kudo, M.; Kawai, M. Structure and electronic state of the TiO_2 and SrO-terminated $SrTiO_3$ (100) surface. *Surf. Sci.* **1993**, *287–288*, 377–381. [CrossRef]
77. Ikeda, A.; Nishimura, T.; Morishita, T.; Kido, Y. Surface relaxation and rumpling of TiO_2-terminated $SrTiO_3$ (001) determined by medium energy ion scattering. *Surf. Sci.* **1999**, *433–435*, 520–524. [CrossRef]
78. Charlton, G.; Brennan, S.; Muryn, C.A.; McGrath, R.; Norman, D.; Thornton, G. Surface relaxation of $SrTiO_3$ (001). *Surf. Sci.* **2000**, *457*, L376–L380. [CrossRef]
79. Eglitis, R.I.; Popov, A.I. Comparative ab initio calculations for ABO_3 perovskite (001), (011) and (111) surfaces as well as $YAlO_3$ (001) surfaces and *F* centers. *J. Nano Electron. Phys.* **2019**, *11*, 01001. [CrossRef]
80. Borstel, G.; Eglitis, R.I.; Kotomin, E.A.; Heifets, E. Modelling of defects and surfaces in perovskite ferroelectrics. *Phys. Status Solidi B* **2003**, *236*, 253–264. [CrossRef]
81. Eglitis, R.I.; Vanderbilt, D. Ab initio calculations of $BaTiO_3$ and $PbTiO_3$ (001) and (011) surface structures. *Phys. Rev. B* **2007**, *76*, 155439. [CrossRef]
82. Eglitis, R.I.; Vanderbilt, D. Ab initio calculations of the atomic and electronic structure of $CaTiO_3$ (001) and (011) surfaces. *Phys. Rev. B* **2008**, *78*, 155420. [CrossRef]

Institute of Solid State Physics, University of Latvia as the Center of Excellence has received funding from the European Union's Horizon 2020 Framework Programme H2020-WIDESPREAD-01-2016-2017-TeamingPhase2 under grant agreement No. 739508, project CAMART²